# DIFFUSER STUDY ON A SQUARED-BACK AHMED BODY CONSIDERING ILES-SVV

**Filipe Fabian Buscariolo**
Department of Aeronautics
Imperial College London/ USP /McLaren Racing
South Kensington, London SW7 2AZ
f.fabian-buscariolo16@imperial.ac.uk

**Julio Romano Meneghini**
Department of Mechanical Engineering
USP
Av. Prof. Luciano Gualberto, 380 - Sao Paulo
jmeneg@usp.br

**Gustavo Roque da Silva Assi**
Department of Naval Engineering
USP
Av. Prof. Luciano Gualberto, 380 - Sao Paulo
g.assi@usp.br

**Spencer John Sherwin**
Department of Aeronautics
Imperial College London
South Kensington, London SW7 2AZ
s.sherwin@imperial.ac.uk

## ABSTRACT

The Ahmed Body is one of the most studied 3D bluff bodies used for automotive research and was first proposed by Ahmed *et al.* (1984). Due to the variation of the slant angle of the read upper surface, it can generate different flow behaviours, similar to a standard road vehicles. In this study we also use the Ahmed body to evaluate the performance of the introduction of a rear underbody diffuser which are commonly applied in high performance and race cars to improve downforce. As a default body we consider the Ahmed Body with Squared-Back or 0° slant angle to perform a parametric study of the rear diffuser angle. We employing a high-fidelity CFD based on Spectral/hp element discretisation that combines classical mesh refinement with polynomial expansions in order to achieve both better accuracy. The diffuser length was fixed at the same length that the top slant angle has previously been studies of 222mm and the angle was changed from 0° to 50° in increments of 10°. An additional case considering the diffuser angle of 5° was also evaluated. It was observed that peak values for drag and negative lift (downforce) coefficient were achieved at 30° diffuser angle, in which the topology indicates flow fully attached with two streamwise vortical structures, similar to results obtained from Ahmed *et al.* (1984), but in this case with the the body flipped upside down.

## INTRODUCTION

Among all automotive bluff bodies studied in the aerodynamic literature, the most widely studied one is the Ahmed Body. It was first proposed by Ahmed Ahmed *et al.* (1984) and was based on previous geometry proposed by Morel (1978), where the geometry can be changed from a quasi-2D flow to a complex bluff body geometry. The the main dimensions of the body are highlighted on Figure 1. The Ahmed body was designed to have similar shape and features to road vehicles, aiming to reproduce the main flow features such as the frontal stagnation, generation of 3D flow structures, ground effects and well-defined separation points.

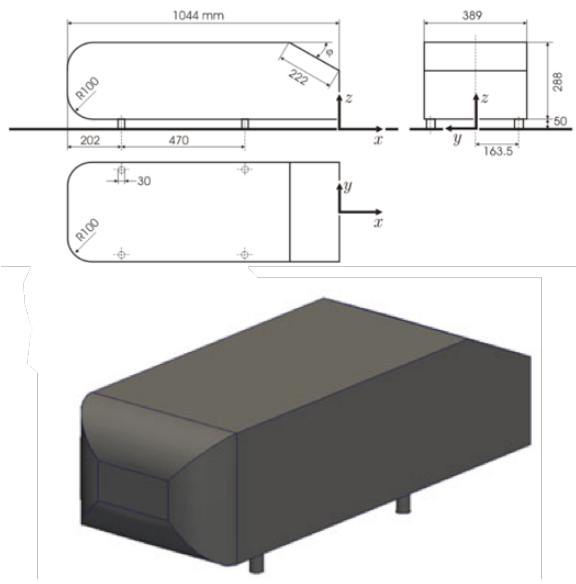


Figure 1: Ahmed Body schematic drawing.

The most emblematic characteristic of the Ahmed Body is a slanted surface on the upper rear portion with fixed length over 21% of the body (i.e.222mm relative to the overall body length of 1044mm). The first experimental study on Ahmed Body Ahmed *et al.* (1984) were with a static floor at a Reynolds number of $Re = 4.29 \times 10^6$ based on the full length. In this study, results for the drag coefficient were obtained for different slant angles, ranging from 0° to 60°, in increments of 10° with an additional measurement at 12.5°. Due to limitations on the wind tunnel setup, only drag force measurements and a few flow visualization test were performed.

Aiming to reproduce the highway conditions and understand the phenomena associated to flow fields close to the ground, Strachan *et al.* (2007) performed an Ahmed

Body wind tunnel test using moving ground and acquired both the aerodynamic forces and the flow characteristics by employing time-averaged LDA. The flow conditions were also slightly different from the ones used on Ahmed's first test, but reducing the Reynolds number to $Re = 1.7 \times 10^6$. Nevertheless, similar flow behaviour were observed on the slant, despite the quantitative results being slightly different. One of the most interesting features found in this flow visualization results is the lower vortex system was a pair of vortices that appears close to the ground interface, which were absent in the fixed-ground studies. According to Strachan *et al.* (2007), this could be attributed to the interference caused by the four studs used to install the model on the floor. Figure 2 illustrates this phenomenon on an Ahmed Body with a squared-back.

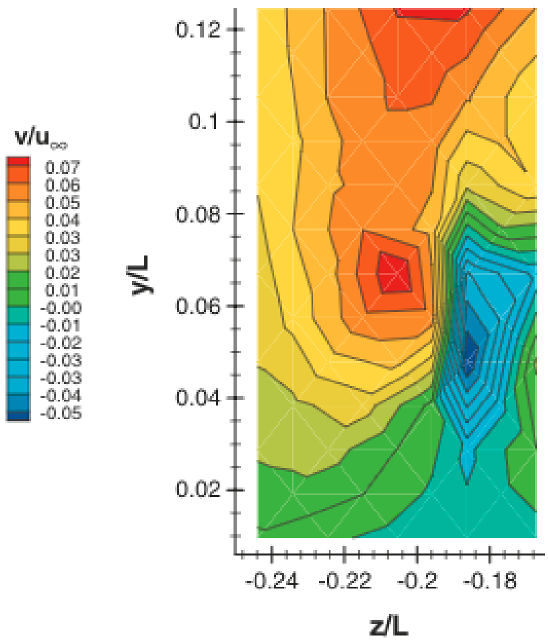


Figure 2: Normalized V velocity on a squared-back Ahmed Body at x/L = 0.048. Reproduction from Strachan *et al.* (2007).

Another development in automotive industry directly associated with the flow near the ground is the introduction of underbody diffusers, initially for high performance race vehicles with relatively low ground clearance. By providing a smoother transition from the underbody flow to the base of the car body, the strength of the rear wake can be reduced, contributing to drag reduction. In addition, it was found that at slightly inclined angles, the underbody diffuser also increases the downforce generated, assisting the acceleration and handling of the vehicle.

Bluff bodies equipped with rear underbody diffusers are being studied by several researchers, especially from the automotive industry, to maximise the performance of the vehicle. The study of Cooper *et al.* (1998) identified three important characteristics on a body underbody diffuser. The first is a diffuser pumping effect, which occurs once the outlet of the diffuser is set as the base pressure of the body, as identified by Jowsey (2013). The diffuser recovers pressure along its length, considering continuity and Bernoulli's equation implies that the diffuser inlet pressure should be reduced, causing the pumping effect. The second characteristic is the interaction with the ground, in which as the ground clearance between the floor and the underbody becomes smaller, it increases the flow velocity in that region by the same continuity and Bernoulli's equation. The flow acceleration reduces the static pressure on the underbody and at the diffuser region, creating an additional suction effect which enhances the diffuser pumping effect. The third characteristic is the angled upsweep, which generates vortices on the diffuser up to a certain critical angle, creating an upwash of the flow, aiding flow attachment and increasing downforce.

Complementing the work of Cooper *et al.* (1998), Senior & Zhang (2001) investigated a new bluff body equipped with a diffuser which extended over 41% of the body length and with inclination angle of 17° and endplates in different ground heights. The result was the identification of four distinct regions of diffuser performance, all related to the model ground height. First region from non-dimensional ride height $h/H$, where $h$ is the distance from the body to the ground and $H$ is the total height of the body, is defined from 0.76 to 0.38 and is defined as downforce enhancement, region where the flow on the diffuser is symmetric with some separation on the diffuser inlet. The second region, referred as maximum downforce, from $h/H$ 0.38 to 0.22, with similar flow behaviour as the first region, except for the formation of a separation bubble at the center of the diffuser. The third and fourth regions are referred both as the downforce reduction and low downforce region from $h/H$ 0.22 where the further ground height reduction also lower the downforce and this fact is explained by the asymmetric and separated flow behaviour at the inlet of the diffuser.

To explore detailed features of the near-ground vortices, and to examine the potential benefits of implementing underbody diffusers, we propose a series of computational study considering same simulation conditions as the experiment from Strachan *et al.* (2007), with moving ground. The base line Ahmed Body considered in the study is the squared-back, representing an estate car (attached flow). In this study, the length of the underbody diffuser is set to be the same as the Ahmed Body slant length, with angles ranging from 10° to 50°, in increments of 10°. An additional case considers diffuser angle of 5°, a setting commonly adopted in race vehicles.

In terms of the methodology for CFD simulations, we selected a high fidelity spectral/hp element simulation using under-resolved direct numerical simulation (uDNS) / implicit large eddy simulation (iLES) approach with sixth polynomial order expansion as in the study of Buscariolo *et al.* (2019). The spectral/hp elemental method combines the properties of spectral and finite element/volume methods, in terms of higher accuracy and rapid convergence, with the geometric flexibility associated with classical h-type mesh refinement Xu *et al.* (2018).

By evaluating the Ahmed Body equipped with a rear underbody diffuser without endplates, we also offer an interesting and simple test case, especially for the squared-back case, as it can be evaluated using a regular Ahmed Body flipped upside-down.

## uDNS/iLES SIMULATIONS USING SPECTRAL/HP ELEMENT METHOD

For the Ahmed body with diffuser, we performed implicit LES simulations based on a spectral/hp element approach. The spectral/hp method first divide the domain into non-overlapping elements, offering geometric flexibility and allowing additional refinement regions. The solution in each element is then approximated by a higher order polynomial expansion. The flow is then solved using an incompressible Navier-Stokes solver using a velocity correction scheme as proposed by Guermond & Shen (2003). The elliptic operators were discretised using a classical continuous Galerkin (CG) formulation. This discretisation was made available through the open source package Nektar++ by Cantwell *et al.* (2015).

Simulation at higher Reynolds numbers, where the flow is typically only marginally resolved, such as the cases here presented typically require careful treatment and some numerical stabilisation. To achieve a more robust and stable solution we therefore employ both dealiasing Mengaldo *et al.* (2015) and spectral vanish viscosity (SVV) Moura *et al.* (2017) stabilization techniques. The SVV is applied to introduce damping on high frequency scales and also to help avoid wave trapping due to mesh expansions.

## SIMULATION METHODOLOGY

We first define the coordinates axis for the cases here presented. In what follows, we use a coordinate system with $X$ as the streamwise direction, $Y$ as the vertical direction and $Z$ as the spamwise direction. The Reynolds number for all simulated cases was $Re = 1.7 \times 10^6$, based on the body total length $L$ of 1044mm and so this reproduces the same conditions employed by Strachan *et al.* (2007). The Ahmed body model is placed on a distance $h$ = 50mm from the ground for both body styles evaluated, as in the original experiment Ahmed *et al.* (1984). Diffuser length $D_L$ is set to the same length of the upper slant $S_L$ of 222mm, without length variation when the inclination angle changes.

The model is positioned so that the rear end of the body was located at $X = 0$ and was in a virtual domain of similar dimensions of the wind tunnel test section size of 1660mm $\times$ 2740mm from the study of Strachan *et al.* (2007). The wind tunnel inlet was positioned at $X = -2L$ and outlet at $X = 2L$ with a total streamwise length of $4L$.

The boundary conditions for the computational study were as follows:

- Ahmed bodies with diffuser are set as wall with no-slip condition;
- A half model of the geometry is used with Symmetry condition imposed at $Z = 0$;
- Uniform velocity profile at the inlet;
- High order outflow condition at the outlet (as proposed by Dong *et al.* (2014));
- A moving ground condition on the floor with speed $U$ in the $X$ direction, as used by Strachan *et al.* (2007).

Simulation were performed for 7 convective time units (CTU) where the free stream flow has advecved a length of 7 $L$. The high-order mesh for all cases presented in this work were generated by the mesh generator module of Nektar++: NekMesh (Turner & Moxey (2017)). We set the boundary layer size of $0.022L$, considering 10 prism layers with growth rate of 1.6. The surface mesh polynomial order was selected to be $6^{\text{th}}$ order for curvature representation. Then using a $6^{\text{th}}$ order polynomial in each spectral/hp element converts a (h)-type mesh with 250,000 elements into 19.8 million degrees of freedom (DOF) per variable.

## RESULTS

### Drag Force Comparison Results

We first present results for the averaged drag force with Figure 3. For the Ahmed Body with squared back, drag force acting over the body initially rises with increasing diffuser angle from 0°, reaching the maximum value at an angle of 30°. Then this trend starts to become reversed for higher angles, indicating saturation of the diffuser efficiency. This finding coincides with the trends observed in earlier studies on Ahmed Body slant angle variations, with the drag breaking point at a similar slant angle (Ahmed *et al.* (1984) and Strachan *et al.* (2007). For all diffuser angles tested, the averaged drag forces are higher than that of the squared-back body without diffuser.

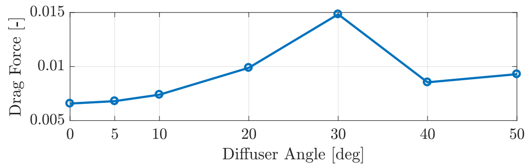


Figure 3: Drag force comparison for Ahmed Body squared-back (blue line) considering standard configuration and evaluated diffuser angles: 5°, 10°, 20°, 30°, 40° and 50°.

### Lift Force Comparison Results

Analyzing the lift force for the Ahmed body squared back, downforce enhancement (or negative lift) is observed as the diffuser angle increases from 0°, reaching maximum downforce at 30°. Again, we observe the breaking phenomenon on downforce for higher diffuser angles, reaching a stable value and following similar trend as the drag force behaviour.

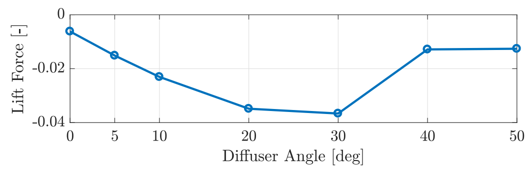


Figure 4: Lift force comparison for Ahmed Body squared-back (blue line) considering standard configuration and evaluated diffuser angles: 5°, 10°, 20°, 30°, 40° and 50°.

The trend break phenomenon observed for both drag and lift coefficients indicates a flow regime change, where the flow structures present on the flow regime present for diffusers up to 30° increase intensity of the downforce up to a saturation point where above this angle, the flow structures on the diffuser change losing its efficiency in terms of downforce. The structures and flow phenomena are discussed as follows.

## Flow Features Analysis

We now present comparative results for the flow structures found on two planes, one at $X/L = 0$, where the end of the Ahmed body is placed and another one further downstream at $X/L = 0.096$, in order to evaluate how the flow structures develop as they separate from the body. From the trends identified in previous drag and lift force analysis, diffuser angles of 20° (DA20), 30° (DA30) and 40° (DA40) were selected, focusing on the flow regime changes. Contours of Q-criterion, $U_x$ (stream wise) and $U_y$ (vertical) velocities are provided aiming to identify vortical structures and define its interactions with the rear wake and rotation direction.

The flow structure on the Ahmed Body squared back with diffuser present has a well-defined behaviour, matching with the quantitative results presented on the drag and lift force comparison. The flow on the diffuser has two different types of behaviours. For diffuser angles up to 30°, the flow is characterized by a pair of counter rotating vortices on the side portion of the diffuser, and separated flow on the middle portion. This is similar to the behaviour observed on the Ahmed Body cases without diffuser, for slant angles ranging from 12.5° to 30°. For diffuser angles above 30°, the flow becomes fully separated.

Both flow regimes are detailed on Figure 5(a), where on plane $X/L = 0$, DA20 and DA30 show the vortex on the outer edge of the diffuser. It's also possible to notice the increment of its intensity from DA20 to DA30. Highlighted on Figure 6(a) is the case considering DA30, with the side vortex moves inwards in the spanwise direction, it interacts with the wake generated from the separation region on the middle portion of the diffuser. The case considering DA40 indicates no vortex generation by the diffuser.

Moving further downstream to plane $X/L = 0.096$, DA 20 and DA40 show similar flow features from the ones highlighted on plane $X/L = 0$. The exception comes from DA30 where Figure 5(b) indicates that the vortex lost its strength, and Figures 6(b) and 7(b) suggest that the turbulent wake generated by the separation on the middle of the diffuser is merging with the vortical structure from the diffuser.

When applying diffuser considering its angle up to 30°, the flow on the region is characterized by a pair of counter rotating vortices, rotating anti-clockwise. We found three different flow regimes on Figure 8: for the 10° and 20° cases, we found the same vortices but with some separation on the diffuser inlet; the case considering diffuser of 30° presented beside the vortex, a separation bubble in the middle of the diffuser, being both phenomena similar to the findings of Senior & Zhang (2001). For the case equipped with diffuser angle of 5°, the vortices are presented without separation on the diffuser inlet. For diffuser cases of 40° and 50°, the flow is fully separated on the diffuser inlet, which explains no increment on downforce.

## CONCLUSION

We presented a computational study on the Ahmed body squared-back equipped with a simplified rear underbody diffuser, representing similar study performed by Ahmed *et al.* (1984) and Strachan *et al.* (2007) considering the original body flipped upside-down. The diffuser length was kept fixed and measurements of drag, lift and flow fields where performed for diffuser angles ranging from 0° to 50°, considering an increment of 10° between the cases and an extra case with an angle of 5°.

The methodology employed an uDNS/iLES simulation considering a high-fidelity spectral/hp element method, which combines both the flexibility of the classical (h)-type methods to correct represent the geometry with the high accuracy and convergence properties of the spectral methods (p). The boundary conditions of the cases are similar to the experiment of Strachan *et al.* (2007), in whiche we selected the incompressible Navier-Stokes solver combined with dealiasing and SVV stabilization techniques.

Results shows that from 0° to 30° there is a trend of both drag and downforce increment, reaching the maximum values for both drag coefficient and negative lift coefficient with the case considering diffuser angle of 30°. After this, there is a break down in both quantities, indicating that diffuser angles of 40° and above present only drag increment without downforce enhancement, comparing with the baseline case without diffuser. The break down is an indication that the flow regime changed on the diffuser region and is confirmed by the flow analysis presented.

Flow regime for diffuser angles up to 30° is dominated by a pair of vortices combined with different flow separation phenomena over the slant. For diffuser angles of 40° and above, flow is fully separated, and both flow regimes explain the drag and lift coefficient trends.

The studies here presented offered interesting results for the study of simplified underbody diffusers on an Ahmed body using a novel iLES-SVV simulation employing spectral/hp element method. This new methodology is being studied in order to master the techniques and offer a reliable methodology for industrial cases in order to have high-fidelity simulations in a feasible running time.

## ACKNOWLEDGEMENT

We should acknowledge, CNPQ for the sponsorship, the HPC facilities at Imperial and also under the UK Turbulence Consortium.

## REFERENCES

Ahmed, S.R., Ramm, G. & Faltin, G. 1984 Some salient features of the time-averaged ground vehicle wake. *Tech. Rep.*. SAE Technical Paper.

Buscariolo, Filipe F, Assi, Gustavo R S, Meneghini, Julio R & Sherwin, Spencer J 2019 Spectral/hp methodology study for iles-svv on an ahmed body. In *Spectral and High Order Methods for Partial Differential Equations ICOSAHOM 2018*, p. to be released. Springer.

Cantwell, C.D., Moxey, D., Comerford, A., Bolis, A., Rocco, G., Mengaldo, G., De Grazia, D., Yakovlev, S., Lombard, J-E., Ekelschot, D. *et al.* 2015 Nektar++: An open-source spectral/hp element framework. *Computer Physics Communications* **192**, 205–219.

Cooper, K.R., Bertenyi, T., Dutil, G., Syms, J & Sovran, G. 1998 The aerodynamic performance of automotive underbody diffusers. *Tech. Rep.*. SAE Technical Paper.

Dong, Suchuan, Karniadakis, George E & Chryssostomidis, C 2014 A robust and accurate outflow boundary condition for incompressible flow simulations on

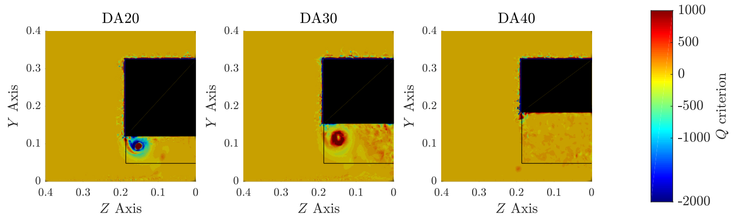


(a) Plane $X/L = 0$

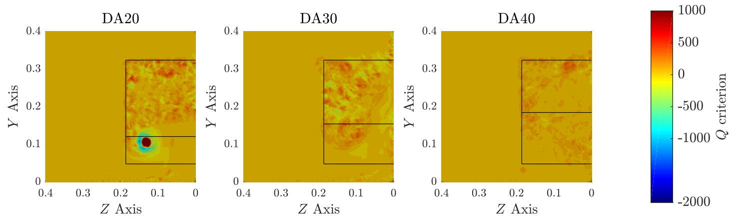


(b) Plane $X/L = 0.096$

Figure 5: Contours of Q-Criterion for the Ahmed body considering diffuser angle of 20° (DA20), 30° (DA30) and 40° (DA40) for plane $X/L = 0$ and $X/L = 0.096$

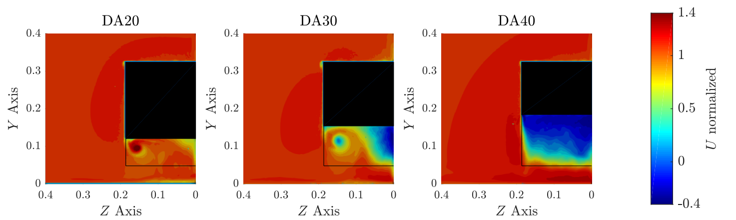


(a) Plane $X/L = 0$

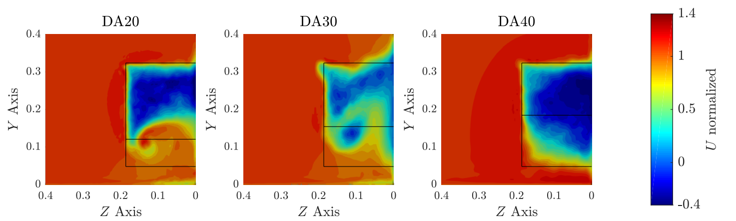


(b) Plane $X/L = 0.096$

Figure 6: Contours of streamwise velocity $U_x$ normalized by the flow velocity $U$ for the Ahmed body considering diffuser angle of 20° (DA20), 30° (DA30) and 40° (DA40) for plane $X/L = 0$ and $X/L = 0.096$

severely-truncated unbounded domains. *Journal of Computational Physics* **261**, 83–105.

Guermond, Jean-Luc & Shen, Jie 2003 Velocity-correction projection methods for incompressible flows. *SIAM Journal on Numerical Analysis* **41** (1), 112–134.

Jowsey, Lydia 2013 An experimental study of automotive underbody diffusers. PhD thesis, © Lydia Jowsey.

Mengaldo, Gianmarco, De Grazia, Daniele, Moxey, David, Vincent, Peter E & Sherwin, SJ 2015 Dealiasing techniques for high-order spectral element methods on regular and irregular grids. *Journal of Computational Physics* **299**, 56–81.

Morel, T. 1978 Aerodynamic drag of bluff body shapes characteristic of hatch-back cars. *Tech. Rep.*. SAE Technical Paper.

Moura, Rodrigo C, Mengaldo, Gianmarco, Peiró, Joaquim & Sherwin, SJ 2017 On the eddy-resolving capability of high-order discontinuous galerkin approaches to implicit les/under-resolved dns of euler turbulence. *Journal of Computational Physics* **330**, 615–623.

Senior, A.E. & Zhang, X. 2001 The force and pressure of a diffuser-equipped bluff body in ground effect. *TRANSACTIONS-AMERICAN SOCIETY OF MECHANICAL ENGINEERS JOURNAL OF FLUIDS ENGINEERING* **123** (1), 105–111.

Strachan, R.K., Knowles, K. & Lawson, N.J. 2007 The vortex structure behind an ahmed reference model in the presence of a moving ground plane. *Experiments in fluids*

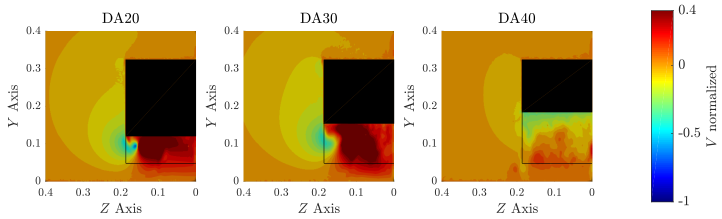

(a) Plane $X/L = 0$

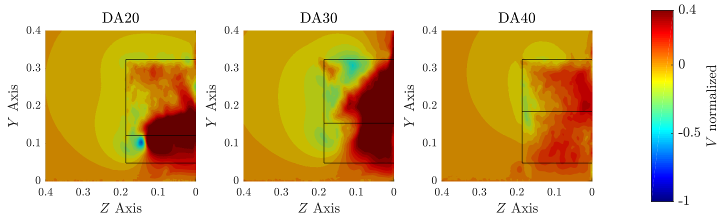

(b) Plane $X/L = 0.096$

Figure 7: Contours of vertical velocity $U_y$ normalized by the flow velocity $U$ for the Ahmed body considering diffuser angle of 20° (DA20), 30° (DA30) and 40° (DA40) for plane $X/L = 0$ and $X/L = 0.096$

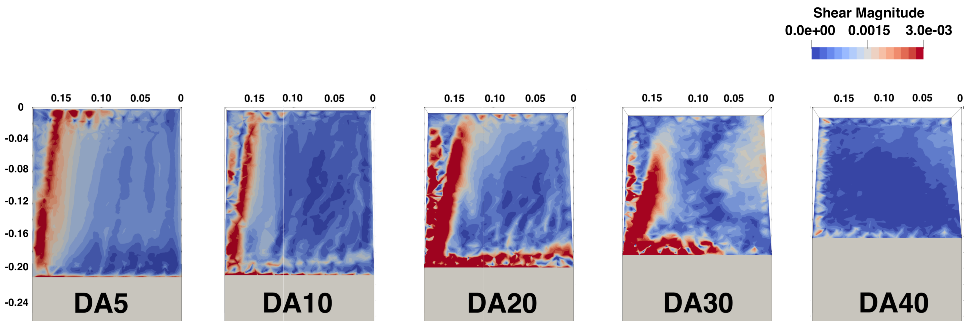

Figure 8: Bottom view of the Ahmed body squared-back presenting contour of shear magnitude on the diffuser angles 5° (DA5), 10° (DA10), 20° (DA20), 30° (DA30) and 40° (DA40), indicating a vortex acting over the diffuser up to DA30 and fully separated flow from DA40 onward.

**42** (5), 659–669.

Turner, Michael & Moxey, D 2017 High-order mesh generation for cfd solvers. PhD thesis, Imperial College London.

Xu, Hui, Cantwell, Chris D, Monteserin, Carlos, Eskilsson, Claes, Engsig-Karup, Allan P & Sherwin, Spencer J 2018 Spectral/hp element methods: Recent developments, applications, and perspectives. *Journal of Hydrodynamics* **30** (1), 1–22.